Synthesis, Characterization and Biological Activity of New Oleander Complexes against Bacteria Found in Polluted Water

Zainab Sabeer Abdulsada[1*], Sahar Sabeeh Hassan[2], and Sanaa Hitur Awad[2]

[1]*Ministry of Environment, Baghdad 10062, Iraq*

[2]*Department of Chemistry, College of Science for Women, University of Baghdad, Baghdad 10071, Iraq*

* ***Corresponding author:***

email:
zainab.sabeer1105a@csw.uobaghdad.edu.iq

Received: May 10, 2023
Accepted: August 11, 2023

DOI: 10.22146/ijc.84332

Abstract: *Natural polymers are often non-toxic, biodegradable, biocompatible, and safe. A novel ligand was synthesized as a natural polymer using chitosan and oleander plant extract [(2R,3S,4R,5S)-5-(acetoxyamino)-4-hydroxy-3,6-dimethoxytetrahydro-2H-pyran-2-yl) methyl (16R)-3-(((2S,4S,5R)-4-methoxy-2,5-dimethyltetrahydro-2H-pyran-2-yl)oxy-10,13,16-trimethyl-17-(5-oxo-2,5-dihydrofuran-3-yl) hexadecahydro-14H-cyclopenta [a] phenanthren-14-yl) phthalate] (Chitosan-Ph-Oleander). This ligand and its complexes with several metals (Cr^{+3}, Mn^{+2}, Fe^{+3}, Ni^{+2}, Cu^{+2}, Zn^{+2}) were characterized using FTIR, UV-visible and ^{1}H-NMR spectroscopy, as well as by molar conductivity, magnetic moment, and TGA analysis. The biological activity for the prepared polymer and its complexes was studied to inhibit the effectiveness of some bacteria found in polluted water taken from hospitals wastewater. The effectiveness of inhibition was tested on* Fusarium oxysporum *fungus, which causes wilting, rotting and seedling death diseases in various types of plants. The elemental and spectral investigation results showed that all prepared compounds had octahedral geometry. Compared to the free ligand, all metal complexes showed discernible antibacterial activity. The zinc(II) complex, in comparison to other metal complexes, showed higher antibacterial activity against* Faecal streptococci *bacteria (G^+) and* Pseudomonas aeruginosa *bacteria (G^-). In addition, the inhibition rate of the effectiveness of the* F. oxysporum *fungus reached ~50%.*

Keywords: *chitosan; contaminated water; inhibiting effectiveness; natural polymer*

■ INTRODUCTION

Biological contaminants including several micro-organisms can interfere the other life forms. The most common transmission mode of these organisms is the fecal–oral pathway, where the major biological contaminants include pathogenic bacteria, coliforms, and *Fecal streptococci* [1-3].

Chitosan is produced by living organisms like fungi and crustaceans (whose shells serve as biomass) [4]. Chitosan is a non-toxic, biocompatible, and biodegradable polymer with antibacterial properties. Chitosan is the second most abundant non-synthetic biopolymer. Most chitosan studies have been used to remediate wastewater [5]. On the other hand, chitosan has been extensively used in synthesis research studies as a functional polymer or a supporting matrix [6]. Amino and hydroxyl groups found in chitosan can interact with the functional groups of the template molecule. However, chitosan's fundamental weaknesses (poor mechanical strength) must be remedied to improve its chemical and physical properties [4]. Recently, chitosan has been used in various studies as an unconventional adsorbent to remove metallic pollutants with high metal adsorption affinities [7-8], as well as for the development of novel materials for wastewater treatment [9].

Apocynaceae is a family of evergreen, lovely flowering shrubs that includes *Nerium oleander*, known as karabi. *N. oleander*'s blooms have four lobes and they are funnel-shaped. They bloom in clusters in terminal branches and are either white or pink. The bark extract

of *N. oleander* has been found to contain a variety of plant secondary metabolites, including steroids, terpenoids, flavonoids, cardenolides, cardiac glycosides, and long-chain esters. Massive biological effects have been noted, including cardiac tonic, diuretic, cytotoxic, antibacterial, anti-platelet aggregation, anti-inflammatory, hepatoprotective, anticancer, anti-hyperlipidemic, anti-ulcer, and anti-depressant action in the central nervous system [10]. Plant extracts are rich in phytochemicals, which operate as reducing and stabilizing agents and demonstrate antibacterial activity against some bacterial and fungal strains. Plant components, including roots, leaves, stems, seeds, and fruits, have also been employed for nanoparticle manufacturing [11]. The plant extracts were economically and environmentally sustainable, opening up new opportunities for water treatment, biosensors, and nanotechnology [12]. The present work described the synthesis of some transition metal complexes using chitosan and oleander plant extract as ligands and then studied the ligand's antibacterial activity and its metal complexes against two types of bacteria found in polluted water.

■ EXPERIMENTAL SECTION

Materials

The oleander leaves were obtained from the University of Baghdad gardens in Al-Jadriya and sent to Ibnu Sina Company in the Ministry of Industry and Minerals to obtain the oleander extract. Chitosan (90%, Glentham, United Kingdom), acetic anhydride (99% B.D.H), phthalic anhydride (99% B.D.H), ethanol (99% B.D.H), and metal salts of ($CrCl_3 \cdot H_2O$, $MnCl_2 \cdot 4H_2O$, $FeCl_3$, $NiCl_2 \cdot 6H_2O$, $CuCl_2 \cdot 2H_2O$, and $ZnCl_2$, B.D.H) were used in this study.

Instrumentation

GMMallen Kampm measured the melting points of the synthesized compounds. MF-370 devised electro-thermal was measured at the University of Baghdad, College of Sciences for Women. SHIMADZU FTIR 8400S Fourier transform within the wavenumber region between 4000 and 400 cm^{-1} using KBr disc and 4000 and 200 cm^{-1} using CsI disc was used to test Fourier transform infrared (FTIR) spectra. The UV-visible spectra at 200–1100 nm were measured using a SHIMADZU 1800 double-beam UV-vis spectrophotometer at the University of Baghdad. ^{1}H-NMR tested using a Bruker Ultra Shield 500 MHz in Tehran University (Iran). Thermal analyses (TGA) of samples were performed under nitrogen atmospheres at a heating range of (0–800 °C) and a heating rate of 20 °C/min using STA500-Germany in Tehran University (Iran). Molar conductivity measurements (μs/cm) out using LASSCO Digital Conductivity Meter for metal complexes (10^{-3} M) in ethanol at room temperature (25 °C). Magnetic moments (eff. B.M) were measured according to Faraday's method using Bruker magnet B.M-6 for the prepared complexes in the solid state at room temperature (25 °C).

Procedure

Synthesis of [(2R,3S,4R,5S)-5-(acetoxyamino)-4-hydroxy-3,6-dimethoxytetrahydro-2H-pyran-2-yl)methyl (16R)-3-(((2S,4S,5R)-4-methoxy-2,5-dimethyltetrahydro-2H-pyran-2-yl)oxy-10,13,16-trimethyl-17-(5-oxo-2,5-dihydrofuran-3-yl) hexadecahydro-14H-cyclopenta[a] phenanthren-14-yl)phthalate]. (Chitosan-Ph-Oleander) ligand

To prepare Chitosan-Ph-Oleander, 2 g (0.0135 mol) of chitosan (off-white color) powder was dissolved in 30 mL of glacial acetic acid (5% v/v) with continuous stirring at room temperature. A solution of 1 M NaOH was added to reach pH 4. In a water bath, 2 mL of acetic anhydride was added and refluxed with continuous stirring at 60–75 °C for 6 h [13].

The second was the reaction of the mixture with 0.827 g of phthalic anhydride dissolved in 10 mL of DMF, for 6 h at 70 °C. In the last step, the product was reacted with 0.7315 g of oleander extract dissolved in ethanol for 6 h at 70 °C. The product was dried at room temperature (25 °C) for a whole night before being washed with diethyl ether (Scheme 1).

Synthesis of Chitosan-Ph-Oleander complexes

The Chitosan-Ph-Oleander complexes were prepared at a ratio of 1:1 from the ligand to the element, whereby 0.1732 g (0.001 mol) of the ligand was dissolved

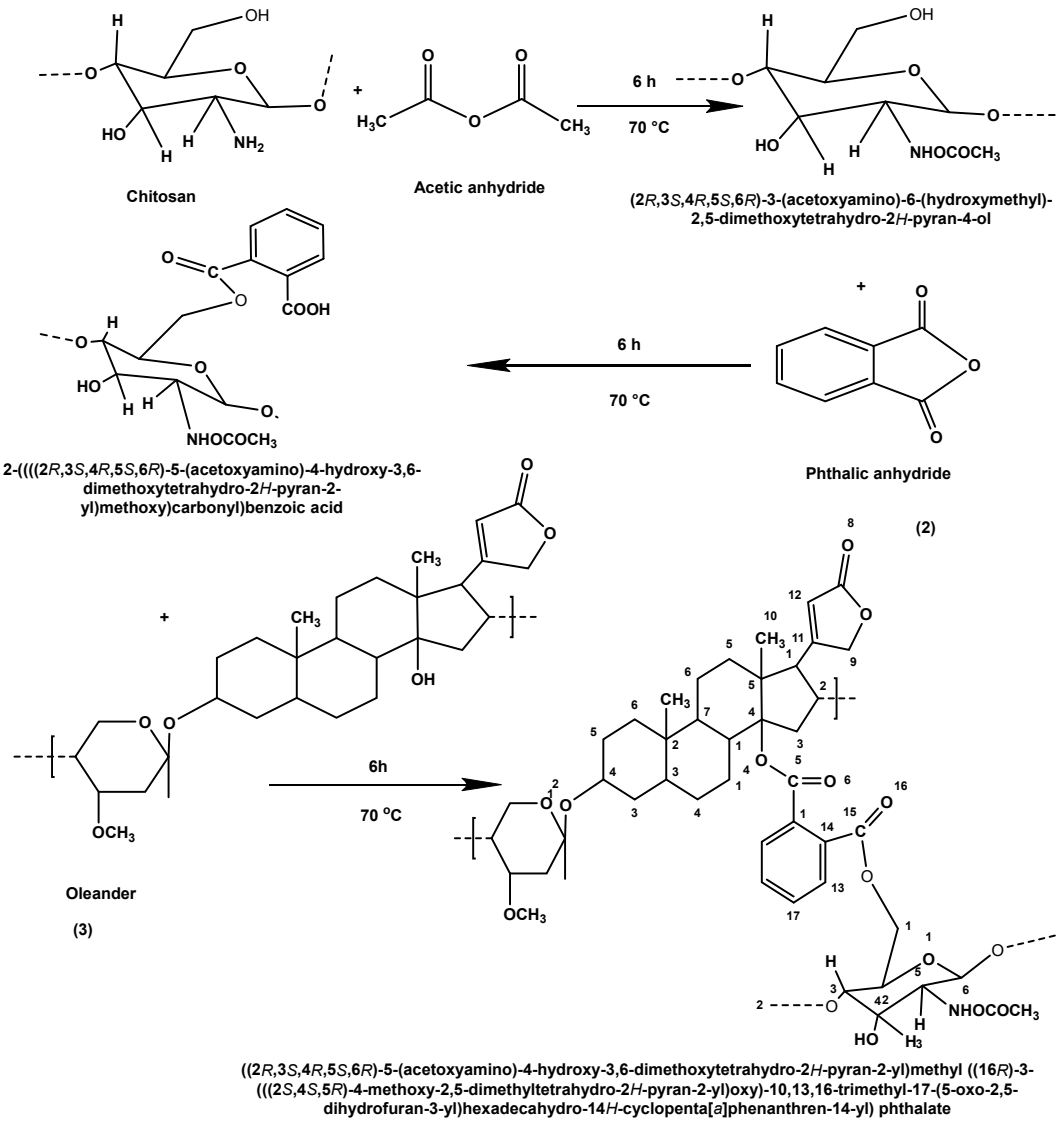

Scheme 1. Preparation of ligand (Chitosan-Ph-Oleander)

in 5 mL of distilled water and 20 mL of absolute ethanol with continuous stirring. Then, the mixture was added by the corresponding weight of 0.001 mol for element salt that dissolved in 10 mL of absolute ethanol with heating at 45 °C for 3 h.

Inhibition activity of ligands and complexes test

In this work, and for studying the biological effectiveness of the compounds that were prepared on each (*F. streptococci* and *P. aeruginosa*) in contaminated water. These compounds were applied using different concentrations (250, 500, and 1000 µg/mL) on each of the bacteria above [12]. The number of bacteria in contaminated water before and after applying these compounds was calculated using the aerobic bacteria total count (ABTC) method.

■ RESULTS AND DISCUSSION

FTIR Spectra of L and Its Complexes

Specific vibrations of chemical bonds or functional groups within molecules appear as FTIR spectra peaks (Fig. 1). KBr in the 4000–400 cm^{-1} and CsI in the 4000–250 cm^{-1} range were used to determine the experimental and theoretical structure of the Chitosan-Ph-Oleander ligand and its complexes. The two absorption peaks at 2819 and 2929 cm^{-1} were due to the asymmetric stretching of chitosan by $-CH_3$ and $-CH_2$, respectively.

Due to –NH symmetry and O–H stretching, the signal at 3433–3176 cm^{-1} in ligand spectra was identified [4].

New bands at 1691–1716 cm^{-1} may be attributed to ν(COO) stretching vibrations [14], whereas bands in the area 3433–3454 cm^{-1} may be assigned to ν(OH) modes. For Chitosan-Ph-Oleander ligand, the bands at 1413 and 1614–1634 cm^{-1} can be attributed to C–N and C=O amide, respectively [15]. The ν(C–N) and ν(C=O) frequencies often rise during complexation. The coordination of the metal ion to the nitrogen of the amide group and the carbonyl oxygen of the carboxylate group could account for these frequency shifts relative to the bands of the ligand. Bands that emerge at 414–487 and 520–597 cm^{-1} were attributed to ν(M–N) and ν(M–O), respectively [16]. The Chitosan-Ph-Oleander ligand appears to behave as a neutral tetradentate ligand, with metal(II) ions bonding through four oxygen atoms, two for the ester carbonyl groups, one for the amide group and one for pyran ring of chitosan (see Table 1, Fig. 1 and 2).

The UV-vis Electronic Spectra of L and Its Complexes

Intense absorption at 277 nm (36101 cm^{-1}) in the UV-vis spectrum of L was ascribed to the n→π* transition, while intense absorption at 206 nm (48543 cm^{-1}) was ascribed to the π→π* transition [17] and three bands appeared for complexes Fig. 3. Table 2 described the physical properties of the ligand and its complexes. Meanwhile, in Table 3, information can be

Table 1. FTIR spectra of the Chitosan-Ph-Oleander and its complexes

Compound	ν(OH)	ν(COO) ester	ν(CO–NH) amide	ν(CH_2–CH)	ν(M–O)	ν(M–Cl)
L	3433	1691	1639	2929 2962	-	
CrL	3444	1704	1614	2929 2860	557	314
MnL	3444	1714	1614	2923 2854	582	324
FeL	3444	1697	1614	2927 2819	580	327
NiL	3454	1716	1614	2925 2856	597	316
CuL	3446	1716	1622	2925 2856	514	316
ZnL	3450	1693	1614	2927 2856	551	312

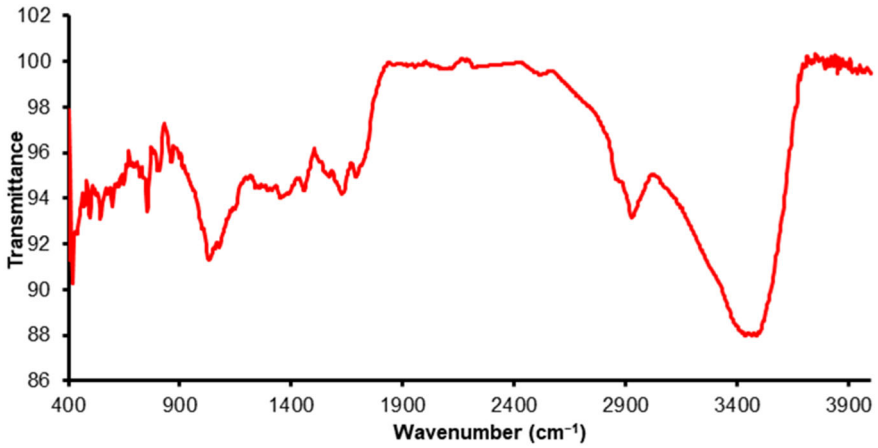

Fig 1. The FTIR spectrum for ligand

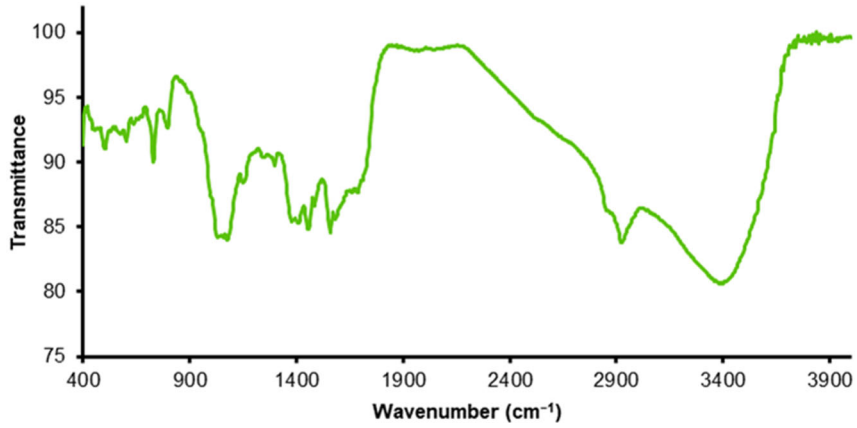

Fig 2. The FTIR spectrum for CuL complex

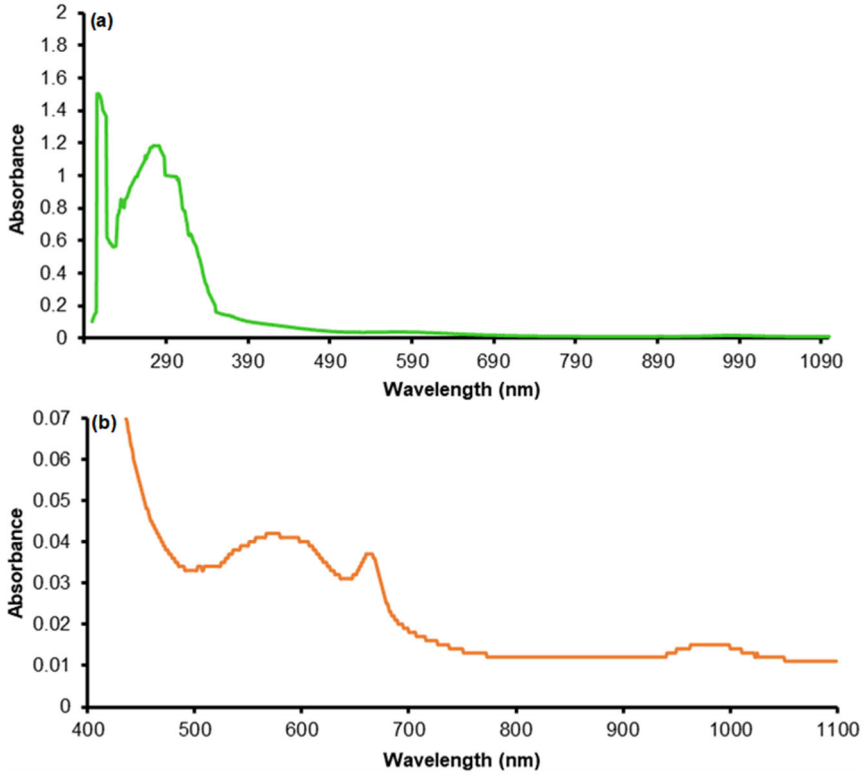

Fig 3. Electronic spectrum of (a) L and (b) CrL complex

Table 2. Physical properties of the ligand and its complexes

Compounds	m.p. (°C)	Color
L	180–182	Greenish brown
FeL	218–220	Yellowish brown
CuL	195–197	Green
MnL	200–202	Light brown
CrL	260–262	Olive
NiL	190–192	Yellowish green
ZnL	210–212	Greenish brown

found on the spectra, magnetic moments, and molar conductivity of all metal complexes of the ligand in ethanol.

Three bands, corresponding to $^6A_1g \rightarrow {}^4T_1g_{(G)}$, $^6A_1g \rightarrow {}^4T_2g_{(G)}$, and $^6A_1g \rightarrow {}^4A_2g+Eg_{(G)}$ were seen for the Mn(II) complex at 664, 606, and 503 nm with 15060, 16501, and 19880 cm^{-1} respectively.

The spectrum of Cr(III) complex olive showed three absorption bands at 978, 664, and 574 nm 10224,

Table 3. The UV-vis electronic spectra, molar conductivity, spectral parameters, and μ_{eff} of L and its complexes

Comp.	Wavelength (nm)	Wavenumber (cm^{-1})	Assignments	Molar cond.	μ_{eff} (B.M)	Structure
L	277	36101	$n\rightarrow\pi^*$	-	-	-
	206	48543	$\pi\rightarrow\pi^*$			
Cr-L	978	10224	$^4A_2g\rightarrow{}^4T_2g$	24.5	3.7	Octahedral
	664	15060	$^4A_2g\rightarrow{}^4T_1g$			
	575	17391	$^4A_2g\rightarrow{}^4T_1g$			
Mn-L	664	15060	$^6A_1g\rightarrow{}^4T_1g_{(G)}$	10.2	5.2	Octahedral
	606	16501	$^6A_1g\rightarrow{}^4T_2g_{(G)}$			
	503	19880	$^6A_1g\rightarrow{}^4A_2g+{}^4Eg_{(G)}$			
Fe-L	966	10351	$^6A_1g\rightarrow{}^4T_1g$	27.5	5.6	Octahedral
	664	15060	$^6A_1g\rightarrow{}^4T_2g$			
	366	27322	$^6A_1g\rightarrow{}^4A_1g+{}^4Eg$			
Ni-L	890	11235	$^3A_2g\rightarrow{}^3T_2g$	7.3	2.3	Octahedral
	662	15105	$^3A_2g\rightarrow{}^3T_1g_{(F)}$			
	450	22222	$^3A_2g\rightarrow{}^3T_1g_{(P)}$			
Cu-L	652	15337	$^2Eg\rightarrow{}^2T_2g$	4.8	1.2	Octahedral
	394	25380	C.T			
	284	35211	Intra ligand			
Zn-L	343	29154	C.T	9.8	Diamagnetic	Octahedral
	218	45871	Intra ligand			

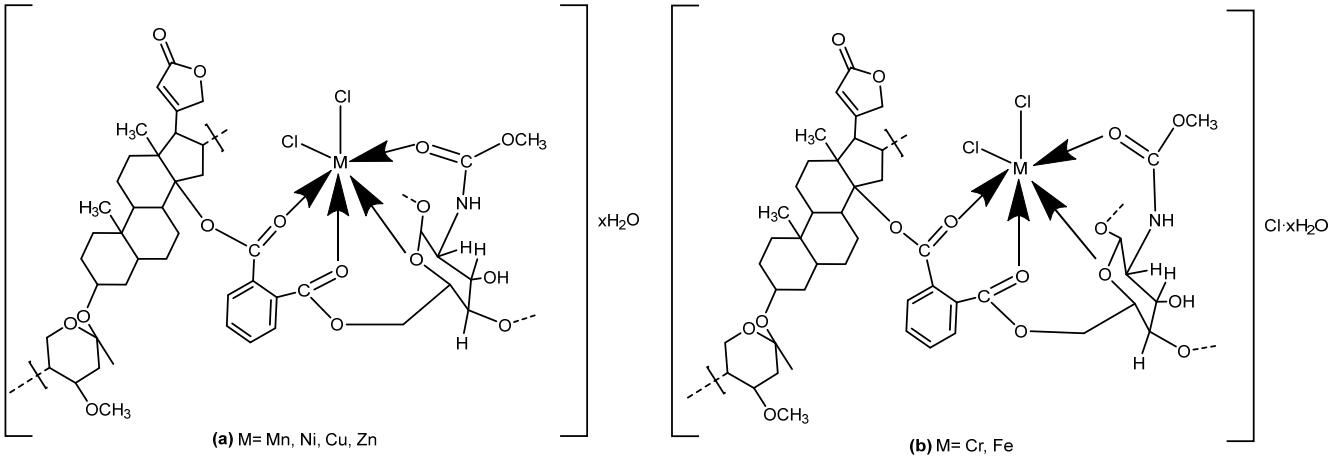

Scheme 2. The geometrical structure of (a) $[MLCl_2]\cdot xH_2O$ and (b) $[MLCl_2]Cl\cdot xH_2O$

15060 and 17391 cm^{-1} assigned to $^4A_2g\rightarrow{}^4T_2g$, $^4A_2g_{(F)}\rightarrow{}^4T_1g$ and $^4A_2g_{(F)}\rightarrow{}^4A_2g$ transitions, suggesting an octahedral geometry. The spectrum of Fe(III) complex showed three bands at 966, 664, and 366 nm, with 10351, 15060, and 27322 cm^{-1} assigned to $^6A_1g\rightarrow{}^4T_1g$, $^6A_1g\rightarrow{}^4T_2g$, and $^6A_1g\rightarrow{}^4A_1g+{}^4Eg$, respectively, suggesting an octahedral geometry; the magnetic moment value is 5.6 BM (Scheme 2(b)). Ni(II) complex spectrum showed three bands at 890, 662, and 450 nm with 11235, 15105, and 22222 cm^{-1} assigned to $^3A_2g\rightarrow Eg$, $^3A_2g\rightarrow{}^3T_2g$, $^3A_2g\rightarrow{}^3T_1g_{(F)}$, and $^3A_2g\rightarrow{}^3T_1g_{(P)}$ transition, respectively. The magnetic moment value was 2.3 BM, suggesting an octahedral geometry (Scheme 2(a)). Cu(II) complex spectrum showed one band at 652 and 394 nm with 15337 and 15380 cm^{-1}, assigned to $^2Eg\rightarrow{}^2T_2g$ and C.T transition, respectively. The magnetic moment value was 1.2 BM suggesting an octahedral geometry [18] (Scheme 2(a)). The magnetic moment value was diamagnetic for Zn(II)

complex, which was attributed to metal-to-ligand charge transfer, but the spectra show no d-d electronic transitions in the visible region. The absorption bands were located at 343 and 218 nm with 29154 and 45871 cm^{-1} assigned to C.T transition and intra ligand, respectively [19] (Scheme 2(a)).

^{1}H-NMR Spectrum

One of the most essential tools for studying substances and their structures is ^{1}H-NMR [20]. The ^{1}H-NMR technique was used to characterize the synthetic polymer and its complexes. Fig. 4 and Table 4 showed that the methylene protons (H, cyclohexyl CH_2) corresponded to a signal at 1.12–1.43 ppm, and a signal at 1.80–2.99 ppm corresponded to methylene and methyl protons [21]. Proton of NH amide was observed at 6.87–7.85 ppm [22]. Amide-containing compounds are among the best examples for clearing the solvent influence on the N–H hydrogen NMR chemical shifts [23]. The protons of the aromatic ring are represented by

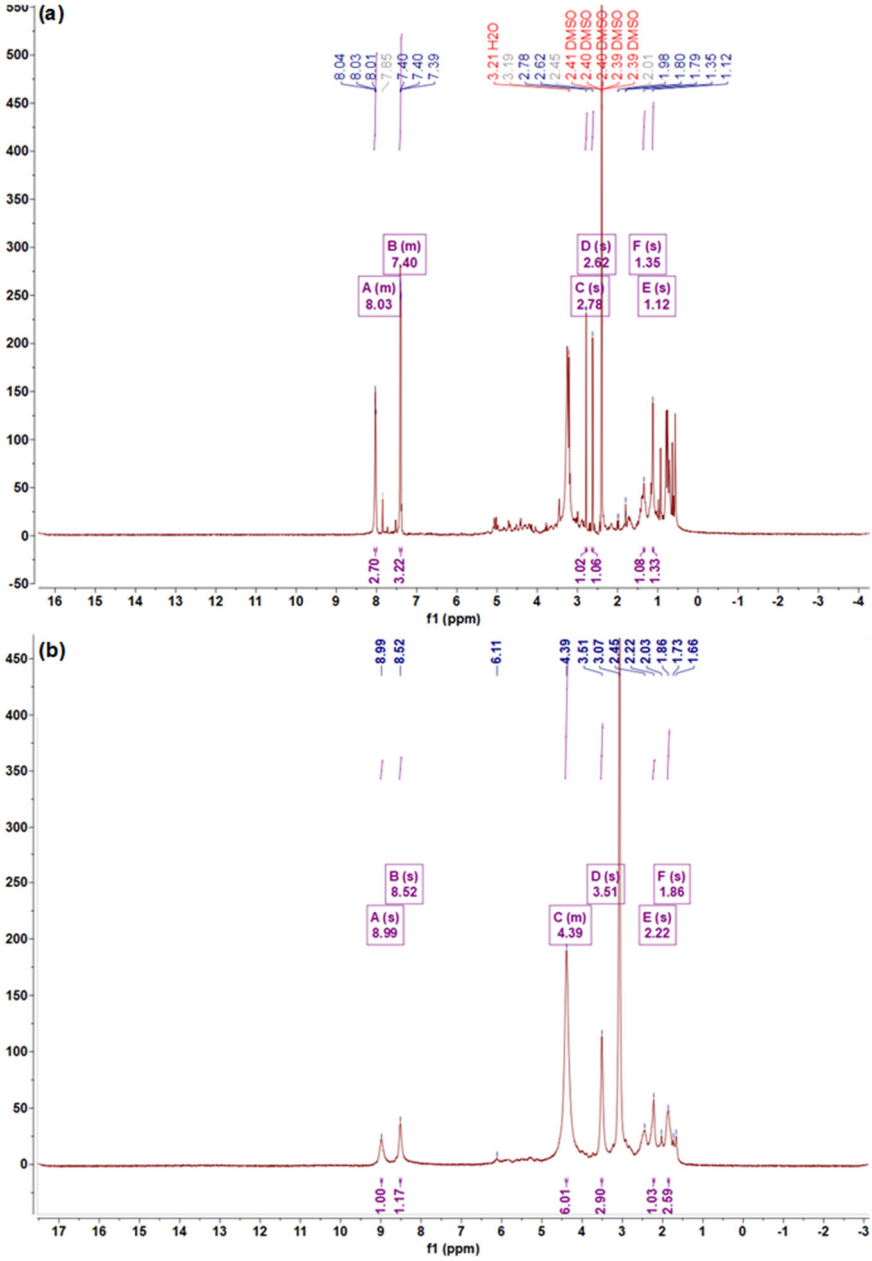

Fig 4. ^{1}H-NMR spectrum of (a) L and (b) FeL

Table 4. ^{1}H-NMR spectral data of L and FeL complex

Chemical shifts (ppm)	Assignments in DMSO
1.12–1.43	Methylene of cyclohexyl protons
1.80–2.99	Methylene and methyl protons
6.87–7.85	Amide proton
8.01–10.09	Hydroxyl group proton
7.38–8.04	Ar–H proton

a multiplet at 7.38 to 8.04 ppm. The spectrum of the CuL and FeL complexes reveal this change to be accurate at the amide group, which gave a signal at 3.25 and 4.17 ppm for these complexes, respectively. Also, it showed a signal for the hydroxyl group at 8.01–10.09 ppm, whereas the methylene proton was represented by 4.40 ppm. CH-aliphatic protons were referred to as a quintet at 4.71 ppm [24].

TGA

TGA was frequently used to understand the effects of temperature and time on the weight of polymeric materials. Polymeric materials can undergo weight changes due to decomposition and oxidation reactions and physical processes, including sublimation, evaporation, and desorption [25]. TGA curves of L and two complexes were illustrated in Fig. 5 and Table 5. The result of ligand presents three stages of weight loss (degradation patterns). Dehydration was the cause of the initial degradation, which begins at 20 °C and lasts until temperatures beyond 150 °C and manifests as a 6.3–8.5% weight loss. The existence of hydrogen bonds between functional groups in both polymer and chitosan and water molecules was the cause of the extended weight loss of water beyond 100 °C. The decomposition of chitosan main chains was responsible for the second weight loss, which starts at about 200 °C and results in a weight loss of roughly 50%. The natural polymer chain remnants go through a third step of decomposition that ranges from 40%. At roughly 800 °C, the ligand and their complexes lose ~85% of their total weight. About 15% of

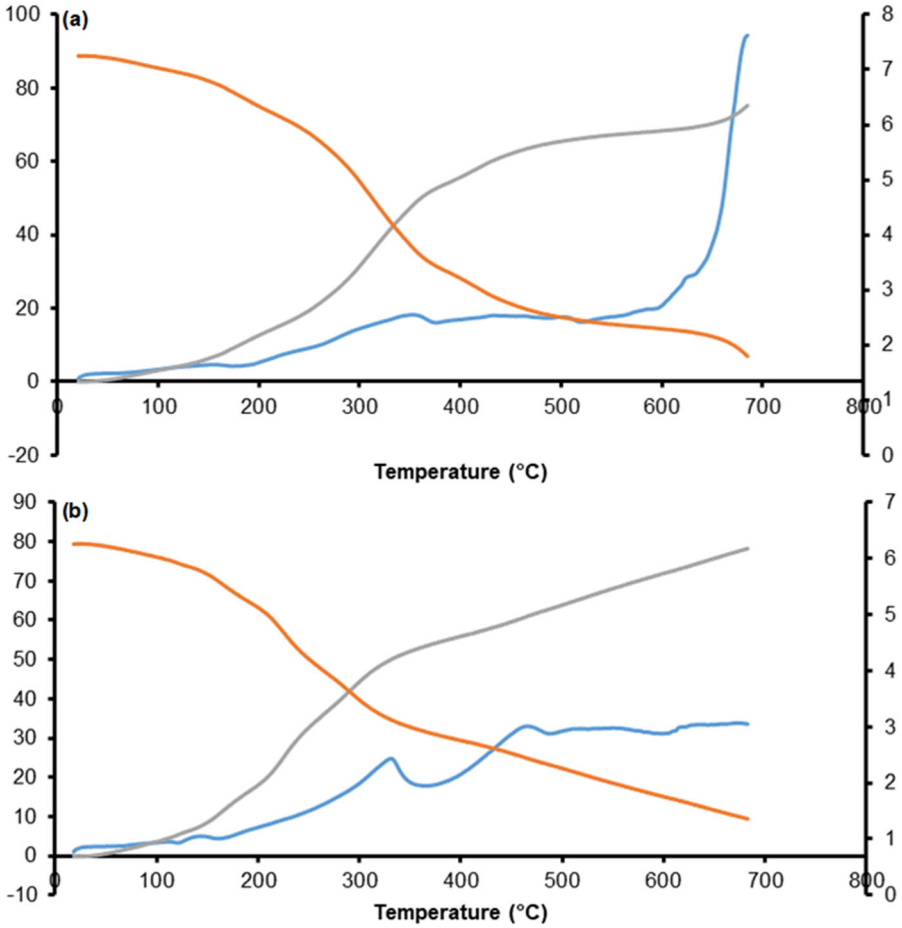

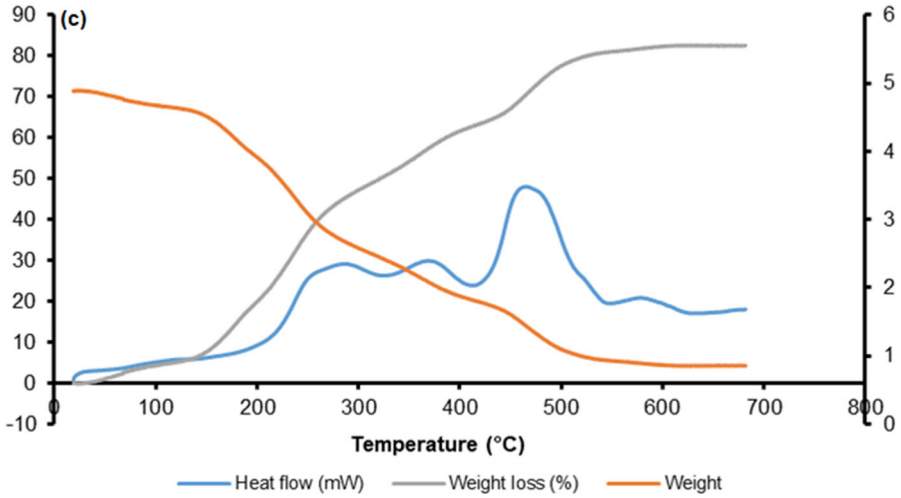

Fig 5. TGA analysis for (a) L, (b) CuL, and (c) FeL

Table 5. Thermal analyses data for L (Chitosan-Ph-Oleander), CuL, and FeL complexes

Compound	Dissociation stages	Temp. range (°C)	Weight loss (%)	Stable phase
L	Stage I	20–150	6.3	Dehydration
	Stage II	200–375	46.2	Chitosan main chains
	Stage III	375–800	38.9	Natural polymer chain residues
$[CuLCl_2]\cdot xH_2O$	Stage I	20–150	8.5	Dehydration
	Stage II	150–340	42.5	Chitosan main chains
	Stage III	340–800	42.5	Natural polymer chain residues
$[FeLCl_3]\cdot xH_2O$	Stage I	20–175	7.5	Dehydration
	Stage II	175–375	50.9	Chitosan main chains
	Stage III	375–800	34.2	Natural polymer chain residues

the compounds were still left over, and this residue was essentially the result of inorganic complexes, including C, N, and O. The literature suggested similar multi-degradation behavior for chitosan [26-28].

Studying of Biological Activity against Bacteria Types Found in Polluted Water

Antibacterial activity

Since human-specific enteric pathogens are more likely to be present in water polluted with human feces than animal feces, this is usually thought to pose a larger risk to human health [29-30]. Fecal waste contamination makes water unsuitable for drinking and contact recreation. Warm-blooded animals' intestines contain naturally occurring bacteria that have been used to detect fecal contamination. At different times, total coliforms, fecal coliforms, and *F. streptococci* have all been utilized as indications of pollution. The Gram-negative, obligatory aerobic, rod-shaped bacteria *P. aeruginosa* is a member of the Pseudomonadaceae family. Although *P. aeruginosa* can develop in several environments, it prefers moist surroundings [31], even though many studies have focused on the characterization of clinical isolates from patients with *P. aeruginosa* infections. Few researchers examined the destiny and incidence of fluoroquinolone-resistant *P. aeruginosa* in clinical wastewater and in the downstream wastewater path [32].

Results of the antibacterial action of ligand and its metal complexes were described, and photographs of growth inhibition zones were illustrated in Fig. 6. Chitosan-Ph-Oleander ligand and its complexes CrL, MnL, FeL, NiL, CuL, and ZnL showed good antibacterial activity at 1000 mg/mL against both bacteria. These findings suggested that, compared to some complexes, the synthesized L showed outstanding activity against the two bacteria under study. Certainly, the mechanism

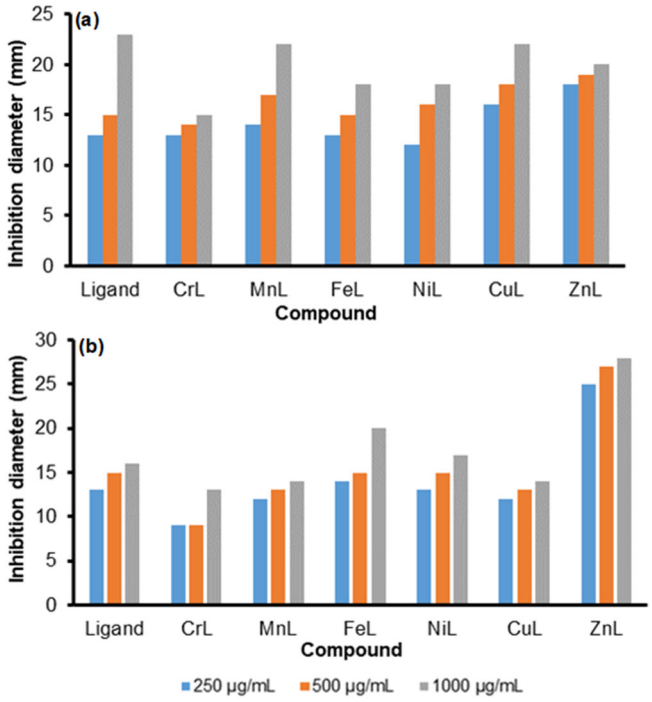

Fig 6. Antimicrobial activity of L and its complexes at 250, 500, and 1000 µg/mL for (a) *Fecal streptococci* and (b) *Pseudomonas aeruginosa*

of chitosan's antibacterial activity was still little understood [33], and three inhibitory mechanisms have thus been suggested. The positive charge amine groups (NH_3^+) of chitosan and the negative charges on the bacterial cell wall were attracted to one another electrostatically in the first mechanism, which prompts the leakage of intracellular components [34].

The second mechanism concerned chitosan's chelating capability toward metal ions such as Ca^{2+}, Mg^{2+}, and Zn^{2+} [35]. In addition to their function in the metabolic pathways, such as spore formation in Gram-positive bacteria, these metal ions were essential for bacterial growth. The third mechanism involves the entry of low-molecular-weight chitosan into the nuclei of microorganisms, which can subsequently interact with DNA, inhibit mRNA expression, and stop protein synthesis, leading to the death of bacterial cells [36].

Among the synthesized series of metal complexes, the MnL and CuL complexes were active against *F. streptococci* bacteria, while ZnL exhibited excellent activity against the two types of bacteria compared to another complex.

Similar observations have been reported by other researchers [37]; for instance, it is well known that both chitosan and Zn have the properties of disinfection and bactericide. After chitosan binds to Zn(II) ions through nitrogen, oxygen, or a combination of them, the bindings are likely to leave some potential donor atoms free, and these free donor atoms enhance biological activity. Thus, it stands a good chance that chitosan–Zn complexes exhibit an enhanced antimicrobial activity, which will be very favorable to chitosan–Zn complexes' applications in the medical and food industries. They investigated the antimicrobial activities of chitosan–Zn complexes and preliminarily explored structure-activity correlation. Five chitosan–Zn complexes with different Zn content were prepared, and their compositions and structures were analyzed through several physical methods. The complexes' antimicrobial activities against four Gram-positive bacteria, five Gram-negative bacteria, and two fungi were studied systematically [38]. Additionally, the ligand and some of its complexes were used in this study to treat dirty water taken from hospital effluent, and they showed high efficacy in removing any number of bacteria found there (Table 6).

Application of the Prepared Ligand and Its Complexes as an Inhibitor for *Fusarium oxysporum* Fungus

Fusarium wilt is the most dangerous and widespread disease in the world, caused by *F. oxysporum*, the main cause of wilting, rotting, and seedling death for more than 100 species of economically important plants. It is one of the fungi isolated from economic crops or soil [39-40]. Several species of Fusarium incite the disease, but the most devastating fungus is *F. oxysporum* [41-42].

The inhibition efficacy of the prepared ligand and its complexes at 250 µg/mL against *F. oxysporum* fungus was studied. Compared to the control, these compounds showed excellent efficacy in inhibiting the growth and activity of this fungus (Table 7). Both Tweedy's chelation theory and the overtone concept can be used to explain the better activities demonstrated by ligands and the inclusion of new complexes [43]. The oxygen that limits the ligand's ability to produce enzymes makes the donor

Table 6. The efficacy of Chitosan-Ph-Oleander Ligand and some of its complexes in removing several bacteria from wastewater

Test	Sample start	L	MnL	NiL
M.P.N of Total *coli* form/100mL	>16000	0	0	0
M.P.N of *Fecal coli* form/100mL	>16000	0	0	0
M.P.N of *E. coli* form/100mL	790	0	0	0
M.P.N of *F. streptococcus* form/100mL	230	0	0	0

Table 7. The antifungal activities of studied compounds (n = 2)

Comp.	Average colony diameter at 250 (µg/mL)	The inhibition percentage (%)
Ligand	4.05	46.60
CrL	3.90	46.60
MnL	3.75	50.00
FeL	3.90	48.00
NiL	3.75	50.00
CuL	3.85	48.60
ZnL	3.75	50.00
Control	7.50	

system more sensitive to metal ions deactivating it during chelation.

Numerous agents could be responsible for the differences in the synergistic effect between the type of metal ion and the associated ligand. The final geometric structure of these complexes, the oxidation state, the species of atoms connected with metal ions, the chelating affinity of the organic molecules utilized as ligands, the coordination number, and the arrangement of the ligand around the central ions are crucial [44]. The chelation mechanism partially shares the positive charge of the metal ion and overlaps the donor group of the ligand orbital, which decreases the polarity of the metal atom and increases the complexes' entry through the lipid layer of the cell membrane. Furthermore, metal complexes impede the cell's ability to respire, obstruct the production of proteins, and stop the organism from growing [45].

■ CONCLUSION

The results showed that the Chitosan-Ph-Oleander ligand and its six metal complexes were synthesized and characterized using various techniques. FTIR, UV-vis and NMR spectroscopy, as well as magnetic moment and conductivity, ensured the formation of compounds. The results explain and ensure metal complexes' geometry and find helpful energy parameters. Furthermore, metal complexes showed an excellent inhibition of two types of bacteria that have all been used as pollution indicators at different times. Results of antibacterial activities revealed that some of these compounds can be used in wastewater treatment or antibiotic development. ZnL, MnL, FeL, and CuL complexes were the most active against these two types of bacteria. In addition, the inhibition rate of the effectiveness of the *F. oxysporum* fungus reached ~50%. Therefore, these results proved the success of the prepared compounds in treating water contaminated with bacteria. Further efforts should be made to explore the possible mechanistic pathways of their activity in wastewater treatment and *in vitro*.

■ ACKNOWLEDGMENTS

The authors acknowledge the staff of the Central Environmental Laboratory in the Ministry of Environment for their assistance.

■ AUTHOR CONTRIBUTIONS

This work has been done by collaboration between all authors. The above part was completed, the vehicles were prepared, the necessary tests were conducted to estimate them, samples were collected, and practical

applications were carried out, in addition to writing the work by Zainab Sabeer Abdulsada, while the work was reviewed and the results checked by Sahar Sabeeh Hassan and Sanaa Hitur Awad.

■ REFERENCES

[1] Aliko, V., Multisanti, C.R., Turani, B., and Faggio, C., 2022, Get rid of marine pollution: Bioremediation an innovative, attractive, and successful cleaning strategy, *Sustainability*, 14 (18), 11784.

[2] Jawad, W.A., Balakit, A.A.A., and Al-Jibouri, M.N.A., 2021, Synthesis, characterization and antibacterial activity study of cobalt(II), nickel(II), copper(II), palladium(II), cadmium(II) and platinum(IV) complexes with 4-amino-5-(3,4,5-trimethoxyphenyl)-4*H*-1,2,4-triazole-3-thione, *Indones. J. Chem.*, 21 (6), 1514–1525.

[3] Fakhriza, M.A., Rusdiarso, B., Sunarintyas, S., and Nuryono, N., 2023, The addition of copper nanoparticles to mineral trioxide aggregate for improving the physical and antibacterial properties, *Indones. J. Chem*., 23 (3), 692–701.

[4] Rahimi, M., Bahar, S., and Amininasab, S.M., 2022, Preparation of molecular imprinted polymer based on chitosan as the selective sorbent for solid-phase microextraction of phenobarbital, *J. Anal. Methods Chem.*, 2022, 9027920.

[5] Mahmoud, R.K., Mohamed, F., Gaber, E., and Abdel-Gawad, O.F., 2022, Insights into the synergistic removal of copper(II), cadmium(II), and chromium(III) ions using modified chitosan based on Schiff bases-*g*-poly(acrylonitrile), *ACS Omega*, 7 (46), 42012−42026.

[6] Rabie, S.T., Mohamed, Y.M.A., Abdel-Monem, R.A., and El Nazer, H.A., 2022, Facile synthesis of chitosan-*g*-PVP/f-MWCNTs for application in Cu(II) ions removal and for bacterial growth inhibition in aqueous solutions, *Sci. Rep.*, 12 (1), 17354.

[7] El-saied, H.A., and Motawea, E.A., 2020, Optimization and adsorption behavior of nanostructured $NiFe_2O_4$/Poly AMPS grafted biopolymer, *J. Polym. Environ*, 28 (9), 2335–2351.

[8] Adel, N., Hassan, S.S., and Awad, S.H., 2021, Green preparation of new nanoparticles composite from chitosan and zeolite to remove excess concentrations of iron and copper from waste water, *J. Green Eng*., 11 (2), 1195–1212.

[9] El Nazer, H.A., and Mohamed, Y.M.A., 2021, "Chalcogenide-Based Nanomaterials as Photocatalysts for Water Splitting and Hydrogen Production" in *Chalcogenide-based Nanomaterials as Photocatalysts*, Eds. Khan, M.M., Elsevier, Amsterdam, Netherlands, 73–183.

[10] Ramadan, R.H., Abdel-Meguid, A., and Emara, M., 2020, Effects of synthesized silver and chitosan nanoparticles using *Nerium oleander* and *Aloe vera* on antioxidant enzymes in *Musca domestica*, *Catrina: Int. J. Environ. Sci.*, 21 (1), 9–14.

[11] Suresh, J., Pradheesh, G., Alexramani, V., Sundrarajan, M., and Hong, S.I., 2018, Green synthesis and characterization of zinc oxide nanoparticle using insulin plant (*Costus pictus* D. Don) and investigation of its antimicrobial as well as anticancer activities, *Adv. Nat. Sci: Nanosci. Nanotechnol.*, 9 (1), 8–16.

[12] Ashwini, J., Aswathy, T.R., Rahul, A.B., Thara, G.M., and Nair, A.S., 2021, Synthesis and characterization of zinc oxide nanoparticles using *Acacia caesia* bark extract and its photocatalytic and antimicrobial activities, *Catalysts*, 11 (2), 1507.

[13] Acemi, A., 2020, Polymerization degree of chitosan affects structural and compositional changes in the cell walls, membrane lipids, and proteins in the leaves of *Ipomoea purpurea*: An FTIR spectroscopy study, *Int. J. Biol. Macromol.*, 16, 715–722.

[14] Ramalingan, A., Kuppusamy, M., Sambandam, S., Medimagh, M., Oyeneyin, O.E., Shanmugasundaram, A., Issaoui, N., and Ojo, N.D., 2022, Synthesis, spectroscopic, topological, Hirschfeld surface analysis, and anti-covid-19 molecular docking investigation of isopropyl 1-benzoyl-4-(benzoyloxy)-2,6-diphenyl-1,2,5,6-tetrahydropyridine-3-carboxylate, *Heliyon*, 8 (10), 10831.

[15] Pihtili, G., Hekim, S., and Pekdemir, M.E., 2022, Molecular structure, vibrational, spectral investigation and quantum chemical DFT calculations of poly(*N*-isopropyl acrylamide-co-nbutyl methacrylate), *Polym. Korea*, 46 (5), 559–565.

[16] Alem, M.B., Damena, T., Desalegn, T., Koobotse, M., Eswaramoorthy, R., Ngwira, K.J., Ombito, J.O., Zachariah, M., and Demissie, T.B., 2022, Cytotoxic mixed-ligand complexes of Cu(II): A combined experimental and computational study, *Front. Chem.*, 10, 1028957.

[17] Al-Bahadili, Z.R., AL-Hamdani, A.A.S., Rashid, F.A., Al-Zubaidi, L.A., and Ibrahim, S.M., 2022, An evaluation of the activity of prepared zinc nanoparticles with extracted alfalfa plant in the treatment of heavy metals, *Baghdad Sci. J.*, 19 (6), 1399–1409.

[18] Hassan, S.S., Hassan, N.M., Baqer, S.R., and Saleh, A.M., 2021, Biological evaluation and theoretical study of bi-dentate ligand for amoxicillin derivative with some metal ions, *Baghdad Sci. J.*, 18 (4), 1269–1278.

[19] Ali, H.R., and Hassan, S.S., 2022, Preparation and study of the physical properties of some complexes with Schiff base ligand for cefdinir derivative, *Iraqi J. Mark, Res. Consum. Prot.*, 14 (2), 110–120.

[20] Baidurah, S., 2022, Methods of analyses for biodegradable polymers: A review, *Polymers*, 14 (22), 4928.

[21] Basri, R., Khalid, M., Shafiq, Z., Tahir, M.S., Khan, M.U., Tahir, M.N., Naseer, M.M., and Braga, A.A.C., 2020, Exploration of chromone-based thiosemicarbazone derivatives: SC-XRD/DFT, spectral (IR, UV-vis) characterization, and quantum chemical analysis, *ACS Omega*, 5 (46), 30176–30188.

[22] Fayyadh, B.M., Abd, N.A.B., and Sarhan, B.M., 2022, Synthesis and characterization of new Mn(II), Co(II), Cd(II) and Hg(II) complexes with ligand [*N*-(pyrimidin-2-ylcarbamothioyl)benzamide] and their antibacterial study, *IOP Conf. Ser.: Earth Environ. Sci.*, 1029 (1), 012030.

[23] Da Silva, H.C., and De Almeida, W.B., 2020, Theoretical calculations of ^{1}H NMR chemical shifts for nitrogenated compounds in chloroform solution, *Chem. Phys.*, 528, 110479.

[24] Sharef, H.Y., and Fakhre, N.A., 2022, Rapid adsorption of some heavy metals using extracted chitosan anchored with new aldehyde to form a Schiff base, *PLoS One*, 17 (9), e0274123.

[25] Dilkes-Hoffman, L.S., Lant, P.A., Laycock, B., and Pratt, S., 2019, The rate of biodegradation of PHA bioplastics in the marine environment: A meta-study, *Mar. Pollut. Bull.*, 142, 15–24.

[26] Elhefian, E.A., Nasef, M.M., and Yahaya, A.H., 2012, Preparation and characterization of chitosan/agar blended films: Part 2., Thermal, mechanical, and surface properties, *E-J. Chem.*, 9, 285318.

[27] Barleany, D.R., Jayanudin, J., Utama, A.S., Riyupi, U., Alwan, H., Lestari, R.S.D., Pitaloka, A.B., Yulvianti, M., and Erizal, E., 2023, Synthesis and characterization of chitosan/polyvinyl alcohol crosslinked poly(*N*-isopropylacrylamide) smart hydrogels via γ-radiation, *Mater. Today: Proc.*, 87 (2), 1–7.

[28] Wang, S., and Xing, Q., 2022, Preparation and *in vitro* biocompatibility of PBAT and chitosan composites for novel biodegradable cardiac occluders, *e-Polym.*, 22 (1), 705–718.

[29] Zhang, Q., Gallard, J., Wu, B., Harwood, V.J., Sadowsky, M.J., Hamilton, K.A., and Ahmed, W., 2019, Synergy between quantitative microbial source tracking (qMST) and quantitative microbial risk assessment (QMRA): A review and prospectus, *Environ. Int.*, 130, 104703.

[30] Abdul Hassan, M.M., Hassan, S.S., and Hassan, A.K., 2022, Green and chemical synthesis of bimetallic nanoparticles (Fe/Ni) supported by zeolite 5A as a heterogeneous Fenton-like catalyst and study of kinetic and thermodynamic reaction for decolorization of reactive red 120 dye from aqueous pollution, *Eurasian Chem. Commun.*, 4, 1062–1086.

[31] Spencer, R.C., 1996, Predominant pathogens found in the European prevalence of infection in intensive care study, *Eur. J. Clin. Microbiol. Infect. Dis.*, 15 (4), 281–285.

[32] Schwartz, T., Volkmann, H., Kirchen, S., Kohnen, W., Schön-Hölz, K., Jansen, B., and Obst, U., 2006, Real-time PCR detection of *Pseudomonas aeruginosa* in clinical and municipal wastewater and genotyping of the ciprofloxacin-resistant isolates, *FEMS Microbiol. Ecol.*, 57 (1), 157–167.

[33] Omer, A.M., Eltaweil, A., El-Fakharany, E.M., Abd El-Monaem, E.M., Ismail, M.M.F., Mohy-Eldin, M.S., and Ayoup, M.S., 2023, Novel cytocompatible chitosan Schiff base derivative as a potent antibacterial, antidiabetic, and anticancer agent, *Arabian J. Sci. Eng.*, 48 (6), 7587–7601.

[34] Li, J., and Zhuang, S., 2020, Antibacterial activity of chitosan and its derivatives and their interaction mechanism with bacteria: Current state and perspectives, *Eur. Polym. J.*, 138, 109984.

[35] Malekshah, R.E., Shakeri, F., Aallaei, M., Hemati, M., and Khaleghian, A., 2021, Biological evaluation, proposed molecular mechanism through docking and molecular dynamic simulation of derivatives of chitosan, *Int. J. Biol. Macromol.*, 166, 948–966.

[36] Helander, I.M., Nurmiaho-Lassila, E.L., Ahvenainen, R., Rhoades, J., and Roller, S., 2001, Chitosan disrupts the barrier properties of the outer membrane of Gram-negative bacteria, *Int. J. Food Microbiol.*, 71 (2-3), 235–244.

[37] Joshi, N.R., Mule, S.G., Gore, V.A., Suryawanshi, R.D., Pawar, G.T., Bembalkar, S.R., and Pawar, R.P., 2022, Synthesis and biological study of novel Schiff base (1-(3-(4-fluorophenyl)-1-isopropyl-1*H*-indol-2-yl)methylene)hydrazine ligand and metal complexes, *J. Explor. Res. Pharmacol.*, 7 (4), 202–207.

[38] Wang, X., Du, Y., and Liu, H., 2004, Preparation, characterization and antimicrobial activity of chitosan-Zn complexes, *Carbohydr. Polym.*, 56 (1), 21–26.

[39] Kavi Sidharthan, V., Aggarwal, R., Surenthiran, N., Pothiraj, G., Kowsalya, P., and Shanmugam, V., 2018, Selection and characterization of the virulent *Fusarium oxysporum* f. sp. *lycopersici* isolate inciting vascular wilt of tomato, *Int. J. Curr. Microbiol. Appl. Sci.*, 7 (2), 1749–1756.

[40] Al-aamel, A.N.A., Al-maliky, B.S.A., 2023, Control pepper fusarium wilting by biocontrol agent *Trichoderma harzianum* and chelated iron Fe-EDDHA, *Baghdad Sci. J.*, In Press.

[41] Rafique, K., Rauf, C.A., Naz, F., and Shabbir, G., 2015, DNA sequence analysis, morphology and pathogenicity of *Fusarium oxysporum* f. sp. *lentis* isolates inciting lentil wilt in Pakistan, *Int. J. Biosci.*, 7 (6), 74–91.

[42] Dongzhen, F., Xilin, L., Xiaorong, C., Wenwu, Y., Yunlu, H., Yi, C., Jia, C., Zhimin, L., Litao, G., Tuhong, W., Xu, J., and Chunsheng, G., 2020, *Fusarium* species and *Fusarium oxysporum* species complex genotypes associated with yam wilt in South-Central China, *Front. Microbiol.*, 11, 01964.

[43] Oyeyinka, S.A., Adepegba, A.A., Oyetunde, T.T., Oyeyinka, A.T., Olaniran, A.F., Iranloye, Y.M., Olagunju, O.F., Manley, M., Kayitesi, E. and Njobeh, P.B., 2021, Chemical, antioxidant and sensory properties of pasta from fractionated whole wheat and Bambara groundnut flour, *LWT*, 138, 110618.

[44] Qasem, H.A., Aouad, M.R., Al-Abdulkarim, H.A., Al-Farraj, E.S., Attar, R.M., El-Metwaly, N.M., and Abu-Dief, A.M., 2022, Tailoring of some novel bis-hydrazone metal chelates, spectral based characterization and DFT calculations for pharmaceutical applications and *in-silico* treatments for verification, *J. Mol. Struct.*, 1264, 133263.

[45] Pasdar, H., Hedayati Saghavaz, B., Foroughifar, N., and Davallo, M., 2017, Synthesis, characterization and antibacterial activity of novel 1,3-diethyl-1,3-bis(4-nitrophenyl)urea and its metal(II) complexes, *Molecules*, 22 (12), 2125.